International Journal of Minerals, Metallurgy and Materials
Volume 25, Number 8, August 2018, Page 922
https://doi.org/10.1007/s12613-018-1641-4

Effects of initial grain size and strain on grain boundary engineering of high-nitrogen CrMn austenitic stainless steel

Zhen-hua Wang[1,2,3], *Jian-jun Qi*[2,3], *and Wan-tang Fu*[2]

1) School of Mechanical Engineering, Yanshan University, Qinhuangdao 066004, China
2) State Key Laboratory of Metastable Materials Science and Technology, Yanshan University, Qinhuangdao 066004, China
3) HBIS Group Technology Research Institute, Shijiazhuang 050023, China
(Received: 8 January 2018; revised: 3 April 2018; accepted: 4 April 2018)

Abstract: 18Mn18Cr0.5N steel with an initial grain size of 28–177 μm was processed by 2.5%–20% cold rolling and annealing at 1000°C for 24 h, and the grain boundary character distribution was examined via electron backscatter diffraction. Low strain (2.5%) favored the formation of low-Σ boundaries. At this strain, the fraction of low-Σ boundaries was insensitive to the initial grain size. However, specimens with fine initial grains showed decreasing grain size after grain boundary engineering processing. The fraction of low-Σ boundaries and the (Σ9 + Σ27)/Σ3 value decreased with increasing strain; furthermore, the specimens with fine initial grain size were sensitive to the strain. Finally, the effects of the initial grain size and strain on the grain boundary engineering were discussed in detail.

Keywords: grain boundary engineering; grain boundary character distribution; grain size; strain; austenitic stainless steel

1. Introduction

Grain boundaries (GBs) significantly affect the bulk properties of polycrystalline materials. Usually, all existing GBs are classified as low-angle GBs (Σ1 boundaries), high-angle special boundaries with ordered and periodic structures (Σ3–Σ29 boundaries), or high-angle general random boundaries [1]. The first two groups are called low-Σ boundaries and have lower boundary energies, particularly Σ1, Σ3, Σ9, and Σ27 boundaries, than those of random high-angle GBs [2]. Grain boundary engineering (GBE) is used to design and optimize the grain boundary character distribution (GBCD) and GB connectivity using low-Σ boundaries [3]. By using GBE, various boundary-related properties are improved, such as ductility during forming [4], intergranular cracking resistance during service [5–6], and resistance to sensitization and intergranular corrosion [7–9]. Therefore, GBE has received considerable attention in the last two decades.

GBE generally comprises thermomechanical processing that constitutes one of the following four categories [1]: one-step recrystallization involving short annealing after moderate-level deformation, iterative recrystallization, one-step strain annealing involving long annealing after low-level deformation, and iterative strain annealing. Different categories suit different metal alloys. GBE is performed to achieve GBs migration and interaction [3,10] and to form a high fraction of low-Σ boundaries. The initial grain size and strain, i.e., the number of GBs and the driving force for GBs migration, are two factors affecting the GB migration rate [11] and GBE.

In terms of grain size, Cao *et al.* [12] reported that coarse-grained structures favor the formation of highly twinned grain-cluster microstructures and improved the GBCD in a nickel alloy. However, Detrois *et al.* [13] observed that when the hot-deformed and recrystallized structure is subjected to further annealing, the recrystallization to finer grain size results in a high fraction of low-Σ boundaries. In terms of strain, in GBE of 321 steel, a 3% pre-strain was found to be most effective [14]. In the GBE of 304 steel, a 5% pre-strain was optimal [15]. In the case of the GBE of Inconel 600 alloy, the fraction of low-Σ boundaries in an 11%

Corresponding author: Zhen-hua Wang E-mail: wangzhenhua@ysu.edu.cn

pre-strained specimen was higher than those observed in 28%, 51%, and 80% strained specimens [16]. However, for the GBE of Incoloy 800H/HT alloy [17], 50% strain was optimal.

The dependence of GBCD on the initial grain size and strain remains unclear; thus, the effects of grain size and strain on GBE were investigated in this study. Thermomechanical processing increases the fraction of low-Σ boundaries in high-nitrogen austenitic stainless steel [18]. Therefore, a high-nitrogen CrMn austenitic stainless steel, 18Mn18Cr0.5N, was selected as the model material. Specimens with grain sizes ranging from 28 to 177 μm were cold rolled to strains of 2.5%, 5%, 10%, and 20%. After annealing, the GBCD was examined via electron backscatter diffraction (EBSD).

2. Experimental

The tested 18Mn18Cr0.5N steel was melted in a vacuum electric furnace and subsequently electroslag remelted. Its chemical composition (wt%) is 0.11 C, 18.46 Mn, 18.5 Cr, 0.54 N, 0.71 Si, 0.02 P, 0.01 S, 0.01 Al, and balance Fe. Slabs were cut from the remelted ingot and subsequently hot rolled at 1000°C to a cumulative strain of ~1.6%. The rolled slabs were held at 1100°C for 5 min, 1100°C for 20 min, 1100°C for 2h, and 1200°C for 3h to achieve grain sizes of 28, 51, 106, and 177 μm, respectively. The materials were machined into cold-rolled specimens that were 10 mm thick, 20 mm wide, and100 mm long. For each grain size, the specimens were cold rolled to 2.5%, 5%, 10%, and 20% engineering strain. Then, the cold-rolled specimens were annealed at 1000°C for 24 h.

The annealed specimens were sectioned vertically to the rolling direction and were subsequently ground and polished. To achieve flat surfaces free from damage, final polishing was performed using a colloidal silica slurry (20 nm). EBSD patterns were evaluated using the TSL–OIM–Analysis software. The specimens were examined using a step size of 2 μm and a misorientation detection limit of 1° (scanning area 1800 μm × 1800 μm). Low-Σ boundaries ($\Sigma \leq 29$) were identified using Brandon's method [19]. Random high-angle GBs were defined as having a misorientation angle greater than 15° without a low-Σ–site lattice coincidence. Low-angle GBs were defined as boundaries with a misorientation of 2°–15°. In the crystal orientation maps, the random high-angle GBs, Σ1, Σ3, Σ9, Σ27, and other low-Σ boundaries were denoted by black, red, white, blue, green, and purple lines, respectively.

Transmission electron microscopy, using a JEM-2010 microscope, was used to examine the deformed microstructure. Hardness measurements were performed using a FM-ARS9000 Vickers hardness testing machine with a load of 9.8 N and a dwell time of 10 s. Ten random points of each specimen were selected for hardness testing.

3. Results and discussion

3.1. Grain boundary character distribution

Fig. 1 shows the typical GBCD of the materials with different grain sizes, where different types of GBs are shown in different colors. The length fractions of Σ1, Σ3, Σ9, and Σ27 boundaries are given. *D* denotes the average grain size without the twin boundaries. The fractions of low-Σ boundaries in the 177, 106, 51, and 28 μm specimens are 58.9%, 58.3%, 63.1%, and 54.5%, respectively.

Fig. 2 shows the typical GBCD after annealing the 2.5% rolled specimens at 1000°C for 24 h. Fine initial grains lead to finer GBE grains, i.e., grains in GBE-processed. The fractions of low-Σ boundaries are similar; for instance, the fractions of Σ3 boundaries are in the range 61.0%–63.1%. In each specimen, typical triple junctions in the GBE-processed materials (i.e., Σ3–Σ3–Σ9 and Σ3–Σ9–Σ27) can be easily identified. Some segments of the random high-angle GBs are replaced by low-Σ boundaries; this type of structure is expected in GBE because low-Σ boundaries inhibit corrosion and crack propagation along random high-angle GBs.

Fig. 3 shows the typical GBCD after annealing at 1000°C for 24 h for the 5% rolled specimens. A large number of low-Σ boundaries are also observed for each specimen, most of which are Σ3 boundaries. The tendency of decreasing GBE grain size with decreasing initial grain size is similar to that observed in Fig. 2. The GBE grains under the 5% strain condition are finer than those under the 2.5% strain condition in specimens with the same initial grain size. The GBE grains in Fig. 3 are nevertheless much coarser than the initial grains, thus suggesting the occurrence of long-distance migration of GBs during annealing.

When the strain was increased to 10%, the fraction of low-Σ boundaries decreased compared to those at 2.5% and 5% strain, particularly in specimens with initial grain sizes of 106, 51, and 28 μm. The fraction of Σ3 boundaries decreased from ~60% to ~50% (Figs. 4(b)–4(d)). Many Σ3 boundaries are straight and neutral [20] and slightly contribute to disrupting the connectivity of the network of random high-angle GBs. Interestingly, the grain size in Fig. 4(a) is finer than the initial size of 177 μm, clearly suggesting that recrystallization occurred during annealing after 10% strain in the 177-μm specimen. Therefore, recrystallization also occurred in the specimens with finer grain structures (Figs. 4(b)–4(d)). However, this fact does not imply that recrystallization did not occur at 2.5% and 5% strain.

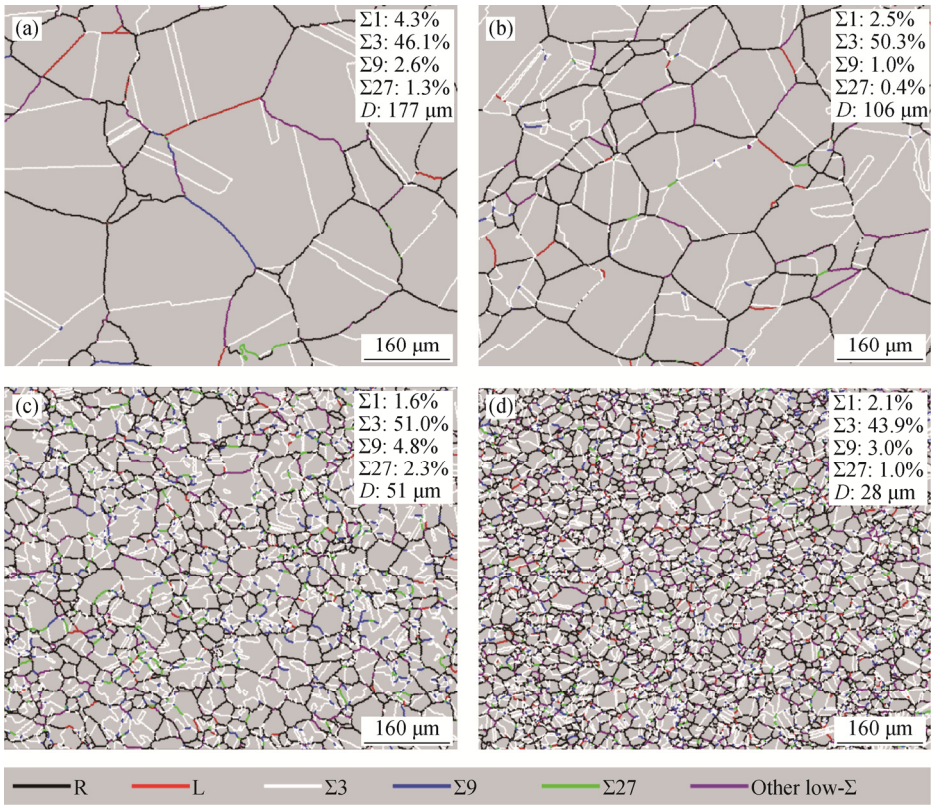

Fig. 1. Orientation imaging microscopy (OIM) maps of specimens with different initial grain sizes: (a) 177 μm; (b) 106 μm; (c) 51 μm; (d) 28 μm.

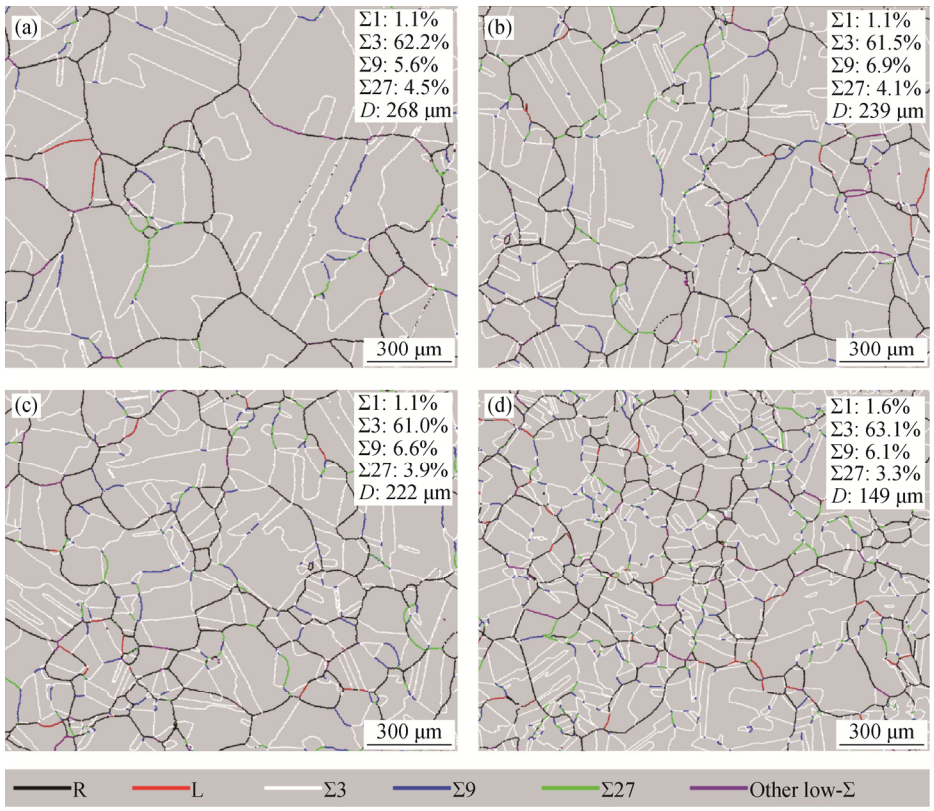

Fig. 2. OIM maps of specimens with different grain sizes at 2.5% strain after annealing at 1000°C for 24 h: (a) 177 μm; (b) 106 μm; (c) 51 μm; (d) 28 μm.

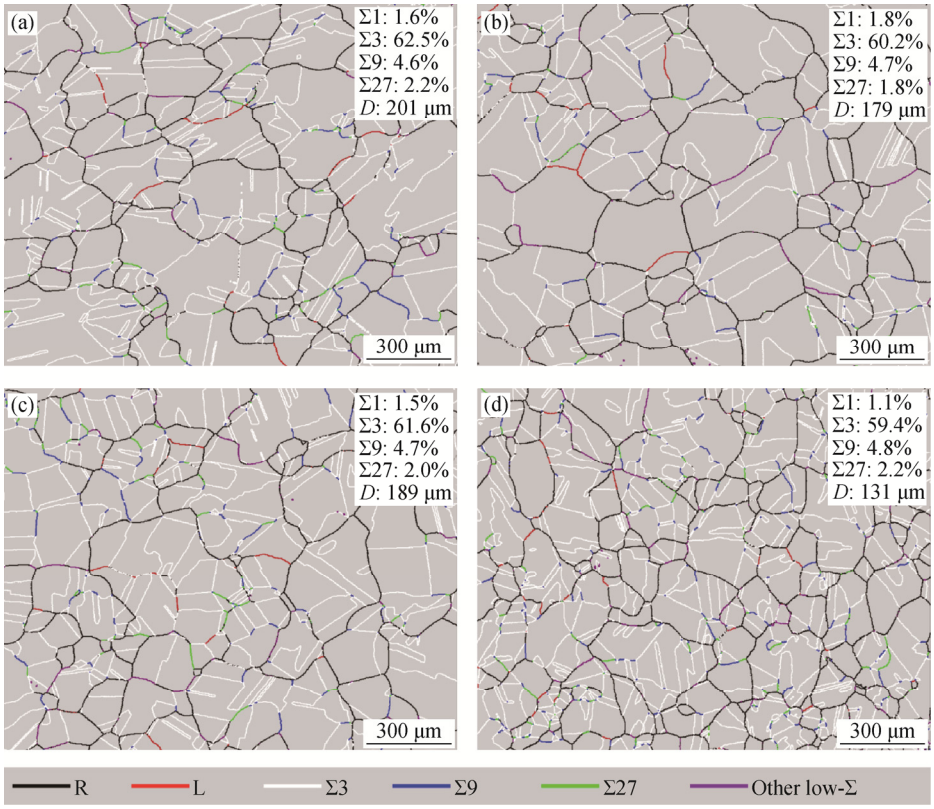

Fig. 3. OIM maps of specimens with different grain sizes at 5% strain after annealing at 1000°C for 24 h: (a) 177 μm; (b) 106 μm; (c) 51 μm; (d) 28 μm.

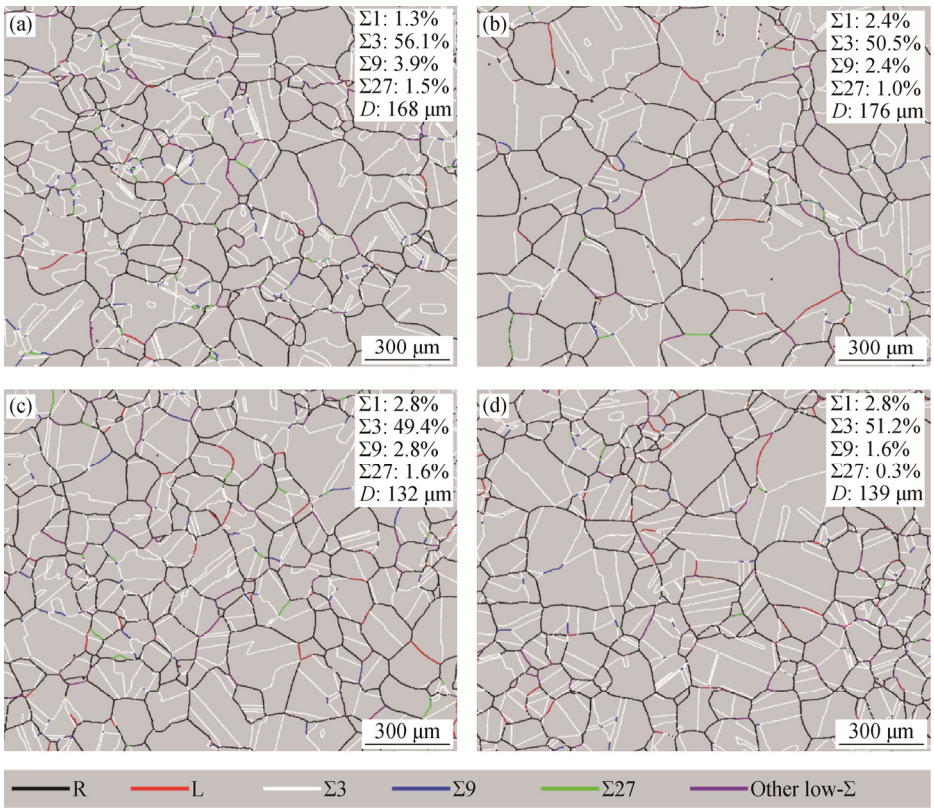

Fig. 4. OIM maps of specimens with different grain sizes under 10% strain after annealing at 1000°C for 24 h: (a) 177 μm; (b) 106 μm; (c) 51 μm; (d) 28 μm.

Fig. 5 shows the typical GBCD after annealing at 1000°C for 24 h for the 20% rolled specimens. A high level of cold rolling evidently produced a small fraction of Σ3 boundaries. The grain sizes in Figs. 5(b)–5(d) are larger than those in Fig. 5(a).

The fractions of low-Σ boundaries under different deformation conditions are shown in Fig. 6(a). In the 2.5% strained specimens, the fractions of low-Σ boundaries are ~75% and insensitive to the initial grain size. It is evident that 2.5% strain and subsequent annealing significantly increased the fraction of low-Σ boundaries. Upon increasing the strain to 10%, the fractions of low-Σ boundaries in the specimens with initial grain sizes of 177, 106, and 51 μm gradually decreased, while the grain size of the 28-μm specimens decreased rapidly. This suggests that specimens with fine grain sizes are more sensitive to strain when subjected to GBE than those with coarse grain sizes. For strains of 2.5%–20%, the low-Σ boundaries decreased by ~20%. The relationship between the (Σ9 + Σ27)/Σ3 and initial grain size and strain is plotted in Fig. 6(b). High (Σ9 + Σ27)/Σ3

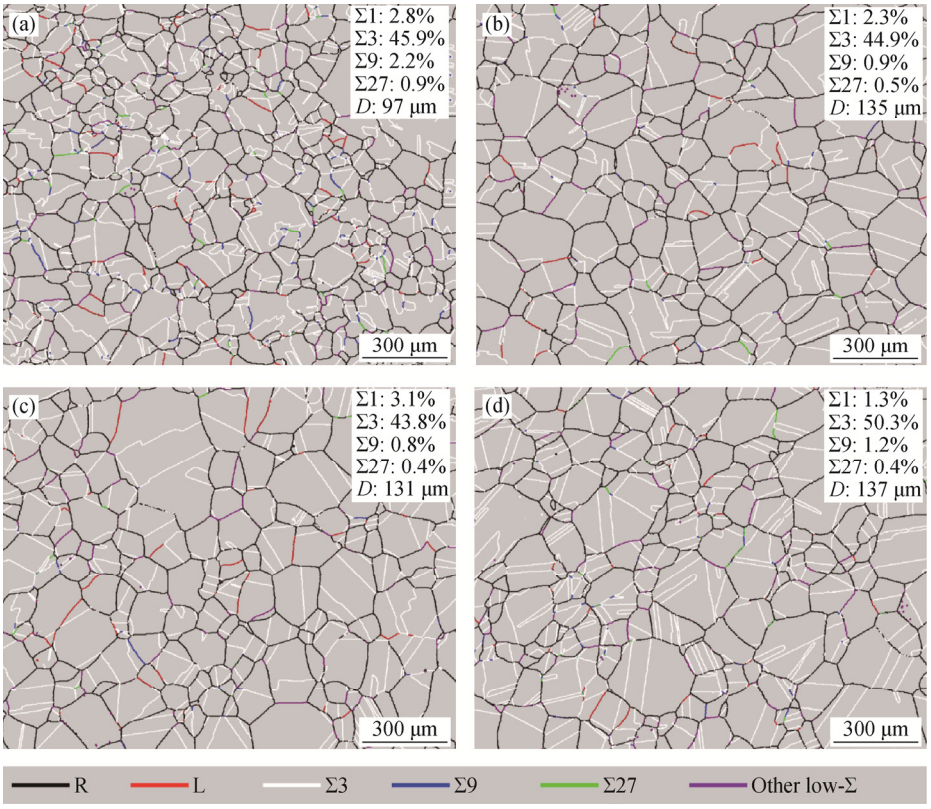

Fig. 5. OIM maps of specimens with different grain sizes under 20% strain after annealing at 1000°C for 24 h: (a) 177 μm; (b) 106 μm; (c) 51 μm; (d) 28 μm.

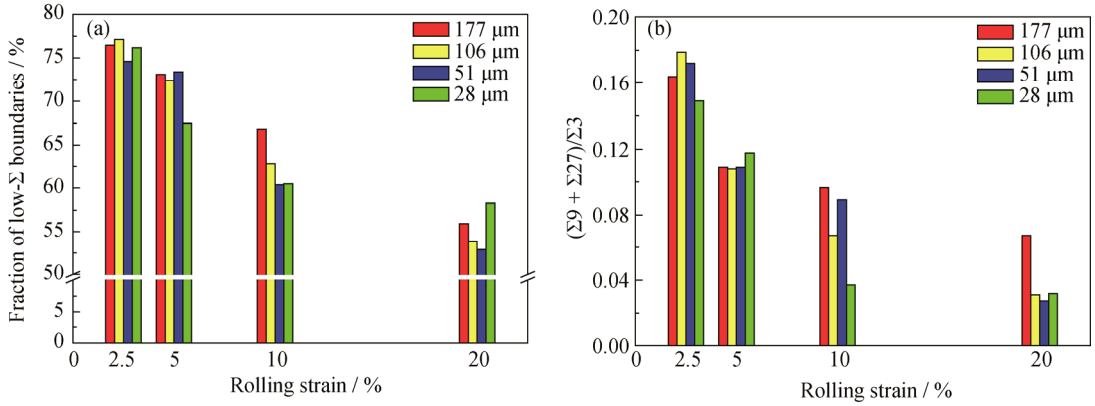

Fig. 6. Fraction of low-Σ boundaries (a) and (Σ9 + Σ27)/Σ3 values (b) under different deformation conditions.

suggests that the low-Σ boundaries form through boundary reactions [17,21] and disrupt the connectivity of random boundaries. In all specimens, high strains clearly result in low (Σ9 + Σ27)/Σ3 values. The decrease in (Σ9 + Σ27)/Σ3 occurs rapidly in the 28-μm specimen.

3.2. Effects of strain and initial grain size

The data presented in Figs. 2–6 shows that the initial grain size and strain considerably affect the GBCD in 18Mn18Cr0.5N steel. A lower strain is beneficial to GBE in 18Mn18Cr0.5N steel based on the fraction of low-Σ boundaries and (Σ9 + Σ27)/Σ3 value. In addition, specimens with fine initial grain sizes are more sensitive to strain than those with coarse initial grain sizes. The effects of strain and initial grain size on GBE are discussed in detail below.

In GBE, long-distance migration of GBs [3,10], which induces GB reactions and the regeneration of low-Σ boundaries, is expected. In the "Σ3 regeneration model," the controlling factors are the impingement of two grains with Σ3 boundaries and the formation of Σ3–Σ3–Σ9 triple junctions [1]. GBs migrate to reduce the total interfacial energy, residual strain energy after recrystallization, and initial cold-strain energy. In other words, in GBE, the primary factor responsible for GB migration should first be induced.

As reported in Ref. [22], a 3% cold strain did not affect the misorientation angle of most of the coincident site lattice boundaries. Subsequently, in annealing, heterogeneous grain growth occurred and grain clusters, i.e., twin-related domains, were formed. The key criterion is that the strain must be sufficiently high to guide the GB migration but not considerably high to destroy the existing low-Σ boundaries, particularly the Σ3 boundaries. Under this condition, the total number of low-Σ boundaries after GBE is approximately the sum of the primary number and the regenerated number.

Fig. 7 shows the microstructure of 18Mn18Cr0.5N steel after 5% cold rolling. Dislocations accumulate at a twin boundary, and the local misorientation angle probably is affected, as indicated by white arrows. In addition, the strain distribution is uniform under high strain conditions [23], which is detrimental to the heterogeneous grain growth and twin-related domain formation during annealing [14–16,22]. These results can explain the reason for which the 5% strained specimens have lower fraction of low-Σ boundaries than the 2.5% strained specimens.

High-nitrogen CrMn austenitic stainless steels are nickel-free engineering materials with interesting mechanical, chemical, and physical properties [8,18,23]. The N concentration exceeds ~0.4wt%. A 2.5% pre-strain was found most effective in 18Mn18Cr0.5N steel. However, the optimal pre-strains in 321 and 304 austenitic stainless steels are 3% and 5%, respectively [14–15]. This difference may be caused by the differences in the stacking fault energies [24].

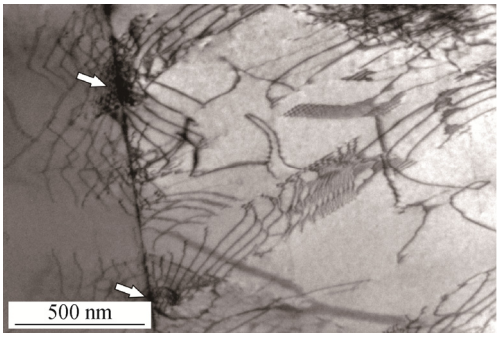

Fig. 7. Microstructure of 18Mn18Cr0.5N steel after 5% cold rolling.

Both random high-angle GBs and Σ3 boundaries are effective barriers to plastic flow [25]. The fine initial grain size leads to high strain hardening rates during cold deformation [26–27]. These findings suggest that an increase in strain will more remarkably change the accumulated strain energy and the uniformity of strain distribution in materials with a finer grain size. Fig. 8 shows the hardness of strained specimens with different grain sizes after rolling. In the strain range of 2.5%–10%, the 28-μm specimen clearly exhibits the highest rate of increase in hardness, which explains reason for the increased strain sensitivity of the material with a fine grain size (Fig. 6).

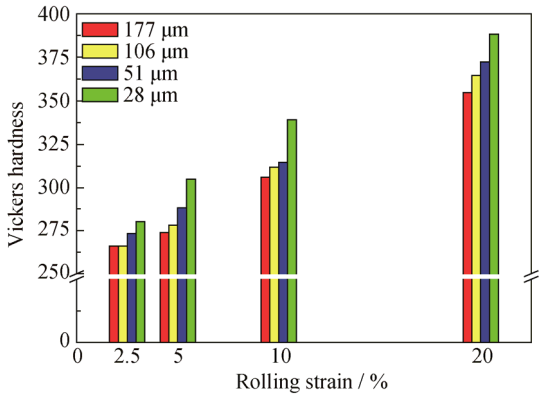

Fig. 8. Hardness of strained specimens with different grain sizes after cold rolling.

The data in Fig. 2 shows that the fractions of low-Σ boundaries are at similar levels in coarse- and fine-grained materials but that the GBE grain size is finer in the latter under 2.5% strain condition. Fine-grained materials contain more GBs than coarse-grained materials; thus, the migration distance of GBs to achieve Σ3 regeneration is small. In addition, the migration occurred in many locations, i.e., the

strain energy is consumed by more growing grains. Hence, the grain size is finer in Fig. 2(d) than in Figs. 2(a)–2(c).

4. Conclusions

Microstructure characterization performed by EBSD elucidated the effect of initial grain size and strain in the GBE of 18Mn18Cr0.5N steel. The following conclusions were drawn.

(1) Low strain (2.5%) favors the formation of low-Σ boundaries.

(2) The fraction of low-Σ boundaries is insensitive to the initial grain size at low strain; however, specimens with a fine initial grain size result in increasingly fine GBE grains.

(3) The fraction of low-Σ boundaries and (Σ9 + Σ27)/Σ3 value decreases with increasing strain, and the specimens with fine initial grain sizes are increasingly sensitive to strain.

Acknowledgements

This work was financially supported by the National Natural Science Foundation of China (No. 51505416), the Natural Science Foundation—Steel and Iron Foundation of Hebei Province, China (No. E2017203041), the Natural Science Foundation of Hebei Province, China (No. E2016203436), and the Post-Doctoral Research Project of Hebei Province, China (No. B2016003029).

References

[1] V. Randle, Mechanism of twinning-induced grain boundary engineering in low stacking-fault energy materials, *Acta Mater.*, 47(1999), No. 15-16, p. 4187.

[2] T. Watanabe, Grain boundary engineering: historical perspective and future prospects, *J. Mater. Sci.*, 46(2011), No. 12, p. 4095.

[3] V. Randle, Twinning-related grain boundary engineering, *Acta Mater.*, 52(2004), No. 14, p. 4067.

[4] Z.W. Zhang, W.H. Wang, Y. Zhou, I. Baker, D. Chen, and Y.F. Liang, Control of grain boundary character distribution and its effects on the deformation of Fe–6.5wt.% Si, *J. Alloys Compd.*, 639(2015), p. 40.

[5] S. Kobayashi, T. Maruyama, S. Tsurekawa, and T. Watanabe, Grain boundary engineering based on fractal analysis for control of segregation-induced intergranular brittle fracture in polycrystalline nickel, *Acta Mater.*, 60(2012), No. 17, p. 6200.

[6] S. Kobayashi, T. Maruyama, S. Saito, S. Tsurekawa, and T. Watanabe, In situ observation of crack propagation and role of grain boundary microstructure in nickel embrittled by sulfur, *J. Mater. Sci.*, 49(2014), No. 11, p. 4007.

[7] R. Jones and V. Randle, Sensitisation behaviour of grain boundary engineered austenitic stainless steel, *Mater. Sci. Eng. A*, 527(2010), No. 16-17, p. 4275.

[8] F. Shi, P.C. Tian, N. Jia, Z.H. Ye, Y. Qi, C.M. Liu, and X.W. Li, Improving intergranular corrosion resistance in a nickel-free and manganese-bearing high-nitrogen austenitic stainless steel through grain boundary character distribution optimization, *Corros. Sci.*, 107(2016), p. 49.

[9] E.A. West and G.S. Was, IGSCC of grain boundary engineered 316L and 690 in supercritical water, *J. Nucl. Mater.*, 392(2009), No. 2, p. 264.

[10] T.G. Liu, S. Xia, H. Li, B.X. Zhou, and Q. Bai, The highly twinned grain boundary network formation during grain boundary engineering, *Mater. Lett.*, 133(2014), p. 97.

[11] D. Horton, C.B. Thomson, and V. Randle, Aspects of twinning and grain growth in high purity and commercially pure nickel, *Mater. Sci. Eng. A*, 203(1995), No. 1-2, p. 408.

[12] W. Cao, S. Xia, Q. Bai, W.Z. Zhang, B.X. Zhou, Z.J. Li, and L. Jiang, Effects of initial microstructure on the grain boundary network during grain boundary engineering in Hastelloy N alloy, *J. Alloys Compd.*, 704(2017), p. 724.

[13] M. Detrois, J. Rotella, R.L. Goetz, R.C. Helmink, and S. Tin, Grain boundary engineering of powder processed Ni-based superalloy RR1000: Influence of the deformation parameters, *Mater. Sci. Eng. A*, 627(2015), p. 95.

[14] K. Kurihara, H. Kokawa, S. Sato, Y.S. Sato, H.T. Fuji, and M. Kawai, Grain boundary engineering of titanium-stabilized 321 austenitic stainless steel, *J. Mater. Sci.*, 46(2011), No. 12, p. 4270.

[15] M. Shimada, H. Kokawa, Z.J. Wang, Y.S. Sato, and I. Karibe, Optimization of grain boundary character distribution for intergranular corrosion resistant 304 stainless steel by twin-induced grain boundary engineering, *Acta Mater.*, 50(2002), No. 9, p. 2331.

[16] B. Li and S. Tin, The role of deformation temperature and strain on grain boundary engineering of Inconel 600, *Mater. Sci. Eng. A*, 603(2014), p. 104.

[17] H. Akhiani, M. Nezakat, M. Sanayei, and J. Szunar, The effect of thermo-mechanical processing on grain boundary character distribution in Incoloy 800H/HT, *Mater. Sci. Eng. A*, 626(2015), p. 51.

[18] H. Kokawa, W.Z. Jin, Z.J. Wang, M. Michiuchi, Y.S. Sato, W. Dong, and Y. Katada, Grain boundary engineering of high-nitrogen austenitic stainless steel, *Mater. Sci. Forum*, 539-543(2007), No. 5, p. 4962.

[19] D.G. Brandon, The structure of high-angle grain boundaries, *Acta Metall.*, 14(1966), No. 11, p. 1479.

[20] E.M. Lehockey, A.M. Brennenstuhl, and I. Thompson, On the relationship between grain boundary connectivity, coincident site lattice boundaries, and intergranular stress corrosion cracking, *Corros. Sci.*, 46(2004), No. 10, p. 2383.

[21] S. Mandal, A.K. Bhaduri, and V. Subramanya Sarma, Grain boundary engineering in alloy D9 through thermo-mechanical

processing: influence of process variables and aspects of micro-mechanisms, *Int. J. Adv. Eng. Sci. Appl. Math.*, 2(2010), No. 4, p. 149.

[22] S. Tokita, H. Kokawa, Y.S. Sato, and H.T. Fuji, *In situ* EBSD observation of grain boundary character distribution evolution during thermomechanical process used for grain boundary engineering of 304 austenitic stainless steel, *Mater. Charact.*, 131(2017), p. 31.

[23] Z.H. Wang, X.Z. Ning, Q. Meng, S.H. Sun, and W.T. Fu. A new insight into manufacturing fine-grained heavy retaining rings, *Mater. Des.*, 103(2016), p. 152.

[24] M. Ojima, Y. Adachi, Y. Tomota, Y. Katada, Y. Kaneko, K. Kuroda, and H. Saka, Weak beam TEM study on stacking fault energy of high nitrogen steels, *Steel Res. Int.*, 80(2009), No. 7, p. 477.

[25] V. Randle and M. Coleman, A study of low-strain and medium-strain grain boundary engineering, *Acta Mater.*, 57(2009), No. 11, p. 3410.

[26] H.B. Li, Z.H. Jiang, Z.R. Zhang, and Y. Yang, Effect of grain size on mechanical properties of nickel-free high nitrogen austenitic stainless steel, *J. Iron Steel Res. Int.*, 16(2009), No. 1, p. 58.

[27] J.T. Shi, L.G. Hou, J.R. Zuo, L.Z. Zhuang, and J.S. Zhang, Effect of cryogenic rolling and annealing on the microstructure evolution and mechanical properties of 304 stainless steel, *Int. J. Miner. Metall. Mater.,* 24(2017), No. 6, p. 638.